Audio Engineering Society

Convention Express Paper 114

Presented at the 155th Convention
2023 October 25–27, New York, USA

On the Impact of Neglecting Accurate Sound-Speed Models on the Cylinder Measurement Method for Directivity Balloons

Matteo Desantis[1]

[1]*NEXO-SA, Plailly, France*

Correspondence should be addressed to Matteo Desantis (matteo.desantis@nexo.fr)

ABSTRACT

The far-field acoustical transfer function of an electroacoustic device, such as a loudspeaker, is of fundamental importance in acoustic modelling software to predict the resulting sound field produced by multiple devices in 3D space. This dataset, commonly known as a *directivity balloon*, is usually acquired through time-consuming, sophisticated measurement techniques involving extensive hardware and dedicated post-processing algorithms. Additionally, such dataset is usually compensated for the effect of acoustical propagation to reference the magnitude and phase values to conventional distances. This works investigates the effects of propagation compensation within the cylinder measurement method for directivity balloons, specifically considering the use of improper sound speed values relative to the ambient conditions during the measurement process. The importance of employing environmental parameter-dependent models for the propagation speed of sound in this type of measurement is emphasized, as to maintain high accuracy in the final directivity data phase response.

1 Introduction

The inherent 3D directivity of sound sources is critical for acoustic modeling software to predict the resulting sound field in specific areas accurately, or alternatively to determine the right DSP settings for a particular device [1]. The significance of acquiring accurate, complex-valued acoustical transfer functions measurements of real sources has been underlined from the very beginning of acoustic simulation software development [2], [3], and over the years, standards for high angular and frequency resolution requirements have been established [4], [5]. Usually, those measurements are performed in large anechoic rooms as to elude the effect of reflections; however, several techniques have emerged to obtain direct sound field components even in the absence of free-field conditions [6], [7].

Typically, 3D acoustical measurements of an electroacoustic source aim to obtain complex-valued far-field [6] frequency responses on the surface of a sphere surrounding the loudspeaker. Such measurement datasets, commonly referred to as *directivity balloons*, allow to model the actual devices as point sources with complex directivity [8] at the receiver's distance. However, for sources that are large with respect to the smallest considered wavelength, this necessitates measurement

distances in the order of 5-10 meters, which may not always be practical either in anechoic or standard reverberant rooms. To overcome these limitations, holography techniques [9], [10] could be utilized to extrapolate far-field radiation behavior from nearfield measurements.

Nevertheless, capturing a measurement dataset on the surface of a sphere presents non-trivial difficulties. Various solutions have been proposed to tackle this issue, such as spherical [10] or arched [11] microphone arrays, and single microphone techniques employing turntables with two rotation-axes [7], [12]. More recently, a novel technique has been introduced by Bru [13], which makes use of two microphones and an elevating turntable only. Regardless of the measurement procedure adopted, the contribution of sound propagation is usually removed from directivity balloons using a spherical propagation law. This involves normalizing the magnitude of the dataset to a sphere of unitary radius, while the phase term is usually referenced to 0 meters instead.

Although it is well known that the propagation speed of sound depends on environmental parameters such as temperature [14], the importance of employing accurate sound-speed models with respect to the propagation compensation has not always been highlighted. Previous studies [7] discouraged outdoor measurements due to changes in environmental variables; in [11], a faster measurement setup was developed in order to reduce the impact of temperature variations on the final measurement data, while the effect of temperature gradients within the measurement room was evaluated; in [11] and [15], it was recommended to monitor air temperature variations between measurements, although little attention was given to relative humidity and other ambient factors.

The objective of this paper is to present the errors introduced by neglecting an environmental parameter dependent sound-speed model when computing directivity balloons using the cylindrical method introduced in [13]. In Section 2, a theoretical model that makes use of the directivity represented by balloon datasets with a sound-speed propagation term is introduced. The experimental setup and post-processing required to compute the final balloon dataset are illustrated in Section 3; Section 4 presents the results followed by conclusions in Section 5.

2 Theoretical Model

Assuming that far field conditions (i.e., receiver distances that are large compared to the spatial extent of the source), and free-field conditions are met, the acoustical transfer function p, due to the pressure radiated at any point in space $\vec{r}$ by a loudspeaker located at the origin of a reference frame, can be expressed in the frequency domain and spherical coordinates as [8]:

$$p(r,\theta,\varphi,\omega) = \frac{A(\theta,\varphi,\omega)}{r} e^{-ikr} \tag{1}$$

wherein $r = |\vec{r}|$, $A(\theta,\varphi,\omega)$ is the complex-valued directional factor, known as the far-field directivity, θ and φ denote the elevation and azimuthal coordinates respectively, ω is the angular frequency and $k = \omega/c$ is the wavenumber, given that c represents the propagation speed of sound in the propagation medium (air). By trivial manipulation, the directivity can be rearranged as:

$$A(\theta,\varphi,\omega) = p(r,\theta,\varphi,\omega) \cdot re^{ikr} \tag{2}$$

That is, given a complex pressure value at a specified point in space, the corresponding directivity factor can be obtained by compensating the measured transfer function value for the attenuation and phase-shift introduced by the spherical wave propagator.

To a first approximation, the propagation speed of sound c can be modelled as a temperature-only dependent value, as expressed by [14]:

$$c = 331.4 \cdot \sqrt{1 + \frac{t}{273}} \tag{3}$$

where t represents the ambient temperature in °C. Assuming a temperature value of 20°C, the equation above yields the commonly used, approximated value of 343m/s at *standard ambient conditions* (see for example [16]). More sophisticated models account for the non-ideal gas nature of air, including the contribution of relative humidity levels (RH) [17], and other environmental parameters such as atmospheric pressure and CO_2 concentration [18]. Fig.1 illustrates the variation of the sound speed value while keeping relative humidity and atmospheric pressure as additional parameters. The spreading of the values along the vertical axis, seen as the temperature rises, is due to the variation of RH from 10% to 100% (left graph) and atmospheric pressure from 95kPa to 105kPa (right graph), according to

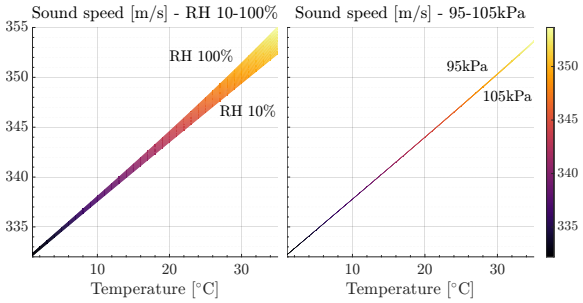

Fig. 1: Sound speed profile as a function of temperature. RH range 10-100% (left), atmospheric pressure range 95-105kPa (right).

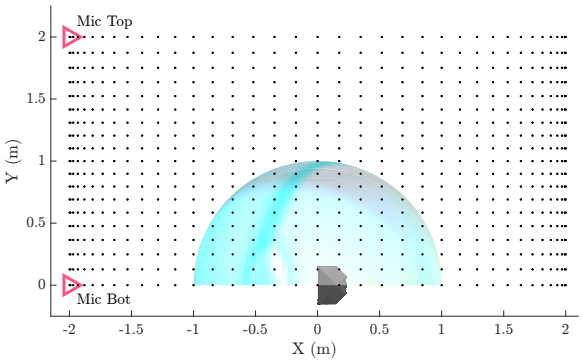

Fig. 2: Positions assumed by the top microphone (black dots) with respect to the loudspeaker in one cylinder measurement. XY plane projection.

the model proposed in [18]; this same model will be employed in the remaining of this paper.

The dependance of the final sound speed value on CO_2 concentration (not shown) and atmospheric pressure appears to be of reduced effect compared to the influence of RH and temperature, therefore the impact due to changes of the first two variables will be neglected in the following. A constant atmospheric pressure value of 1atm = 101.325kPa and a CO_2 molar fraction of 0.0004 will be assumed.

3 Measurement Setup and Post-Processing

The aim of the measurement procedure and further post-processing is to obtain the full audio-range directivity of a loudspeaker on the surface of a sphere of normalized radius. As explained in detail in [13], the balloon is computed from two distinguished anechoic measurement datasets, which are acquired on the surfaces of two orthogonal cylinders. The loudspeaker is located at their center, and in this work the cylinders' radius is constant and set to 2m. The cylindrical measurements are eventually projected on the surface of the sphere, and then interpolated to the desired azimuth and elevation coordinates by means of spherical interpolation techniques [19]. Additionally, a dedicated weighting strategy is applied to penalize the most distant measurement points, which might be more prone to errors due to microphone polar patterns and reduced signal-to-noise ratios.

One advantage of this method, as described in [13], is that only two microphones are required instead of spherical [10] or arched microphone arrays [11]. Furthermore, the loudspeaker needs to be rotated on a single plane only and translated on the direction normal to the rotation plane. Thus, two-axes rotations of the device under test (DUT) are avoided, and the data is acquired in a reduced amount of time compared to one-microphone based techniques [7]. An insight into the cylindrical measurement process is found in Fig.2, wherein black dots represent YZ-plane projections of all the positions assumed by the top microphone on a single cylinder with respect to the center of the loudspeaker's grille. The spherical surface represents the unit sphere, and the projection procedure from one of the cylinders to the unit sphere is illustrated in Fig.3. Some different projection distances $D_{err}(R,h)$ are highlighted by the colored lines.

It follows easily that the terms $d_{err}(R,h) = D_{err}(R,h) - R$ depend on the cylinder radius R and on the height h of the measurement positions. Using a spherical propagator, the compensation factors are given by:

$$E(R,h,\omega,c) = \left[R + d_{err}(R,h)\right] \cdot e^{i\frac{\omega}{c}[R+d_{err}(R,h)]} \quad (4)$$

wherein the dependence of the phase-correction term on the sound speed value has also been made explicit. Fig.4 shows the impact of changes of such value on the phase of the error terms $E(R,h,\omega,c)$ at different heights on the cylinder, compared to what would be obtained if the sound speed was assumed to be fixed at 343m/s. In this example, the temperature is varied from 10°C to 20°C and 30°C and RH is set to 50%. Each group of curves (represented in different colors)

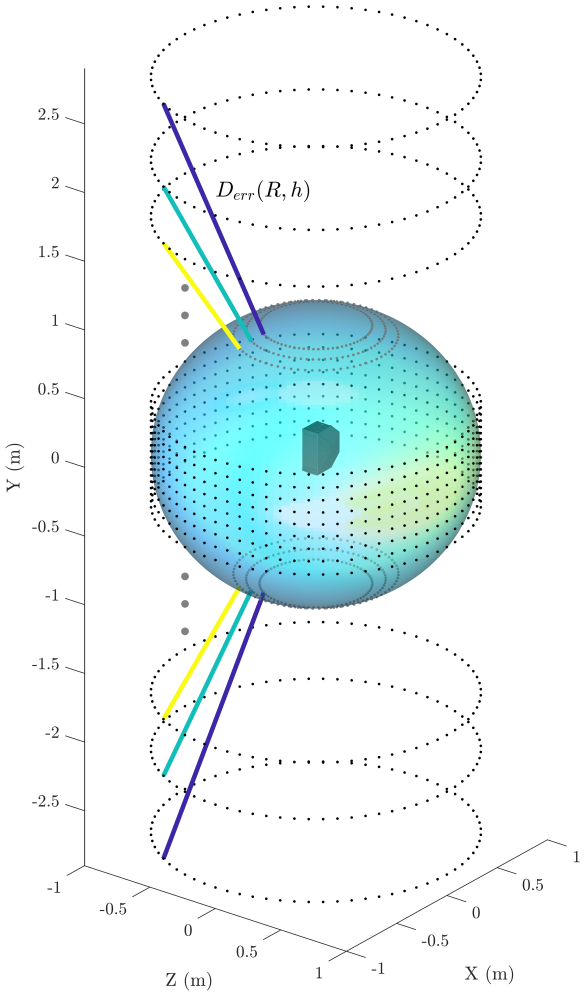

Fig. 3: Projection process from the surface of one cylinder (not in scale) to the unitary sphere. Coloured lines $D_{err}(R,h)$ represent the projection distances (from speaker to sphere hidden).

highlights the spread of the phase errors due to multiple projection distances.

4 Results

All the presented results are obtained from the same initial measurement dataset, consisting of two orthogonal cylindrical measurements of a NEXO ID24 cabinet acquired in the company's anechoic chamber. This speaker has two lines of symmetry perpendicular with each other, lying on a plane normal to the on-axis direction of the cabinet. Therefore, its radiation behaviour

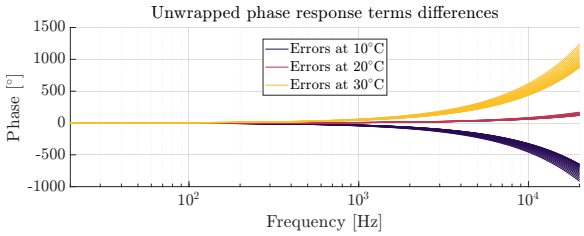

Fig. 4: Changes in the phase shifts introduced by the $d_{err}(R,h)$ terms between a fixed sound speed and a temperature-dependent model.

is equally expected to exhibit symmetry axes on the vertical and horizontal planes.

The measurement data was then post-processed to compute the final directivity balloons. At first, the effect of propagation was compensated at measurement time using the environmental parameter-dependent model. Temperature, RH and atmospheric pressure values inside the anechoic chamber were also acquired throughout the whole measurement process.

Subsequently, alternative configurations of the environmental parameters were defined. Their effect was applied to the compensated cylinders using the spherical propagator with the recomputed sound speed values, as to emulate the measurement process under different conditions.

Finally, the effect of propagation was again removed assuming a fixed sound speed of 343m/s, for all ambient parameters configuration, as to underline the effect of unproper compensation on the processed result. Several scenarios are investigated.

4.1 Both cylinders measured under the same ambient conditions

In this section, the same processing is applied to both the cylindrical datasets, thus assuming that the data acquisition was operated under the same temperature and RH conditions. The effects are evaluated for temperatures of 10°C and 30°C, and for humidity levels of 30% and 70%.

4.1.1 Effect of temperature variations

At first, the simulated environmental parameters were set to 30°C and 50% RH. To evaluate the impact of such changes, the directivity balloon obtained with those

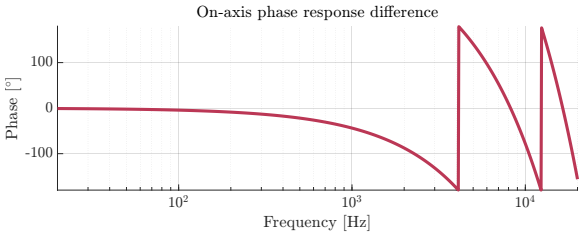

Fig. 5: $\phi_{on-ax}(f)$ difference at 30°C between balloons computed with fixed speed and a temperature dependent model.

parameters was normalized to the dataset compensated using the ambient-dependent model and the ambient parameters' values recorded during the measurement.

The results show that a phase shift is observed on the entire balloon, which can be modelled as:

$$\phi_{tot}(f,\theta,\varphi) = \phi_{on-ax}(f) + \phi_{dir}(f,\theta,\varphi) \qquad (5)$$

wherein the observed phase shift $\phi_{tot}(f,\theta,\varphi)$ is decomposed into a direction-independent, constant term $\phi_{on-ax}(f)$ and a directive component $\phi_{dir}(f,\theta,\varphi)$. Additionally, $\phi_{on-ax}(f)$ can be further expressed as a linear phase term given by:

$$\phi_{on-ax}(f) = -2\pi f t_s \qquad (6)$$

in which $t_s > 0$ represents the time-delay associated with the linear phase shift shown in Fig.5. If the omnidirectional term $\phi_{on-ax}(f)$ is removed from the directivity balloon by means of the complex exponential:

$$\Phi(f) = e^{-i\phi_{on-ax}(f)} = e^{+i2\pi f t_s} \qquad (7)$$

the directional phase error term $\phi_{dir}(f,\theta,\varphi)$ can be highlighted, especially in the very high frequency (Fig.6). The black arrow on the balloon-phase plot represents the on-axis direction of the cabinet.

Similar results can be observed in Fig.7- 8 when the temperature is set to 10°C instead.

It appears clearly that although the entity of the directional dependent phase shift is of reduced amount compared to the omnidirectional component (the latter being non-negligeable), the biggest errors in the directional phase response of the complex directivity balloon are located at the edges of the projected-cylinder datasets, where the distance being compensated is larger. As a mitigating effect, at very high frequencies the cabinet shows high-directivity towards the on-axis direction, which reduces the impact of off-axis phase-inaccuracies.

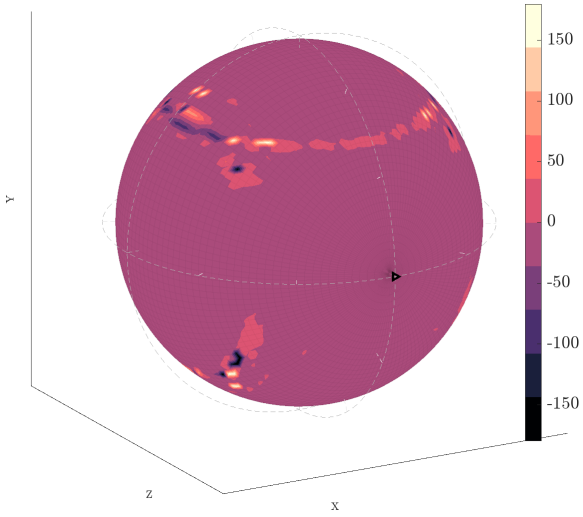

Fig. 6: $\phi_{dir}(f,\theta,\varphi)$ difference at 30°C between balloons computed with fixed speed and a temperature dependent model, f = 16.8kHz.

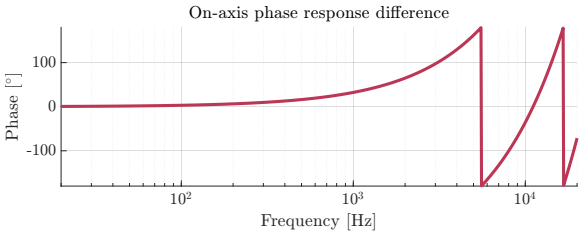

Fig. 7: $\phi_{on-ax}(f)$ difference at 10°C between balloons computed with fixed speed and a temperature dependent model.

4.1.2 Effect of relative humidity variations

As the effect of RH variations is of minor impact on the sound speed model, reduced phase shifts are expected compared to temperature variations. Fig.9 shows the omnidirectional component $\phi_{on-ax}(f)$ for ambient parameters given by 20°C and RH values set to 30% and 70%, compared to what is obtained assuming the sound speed being fixed to 343m/s.

Considerations regarding the directional term $\phi_{dir}(f,\theta,\varphi)$ with respect to RH changes are akin to those mentioned in the case of temperature variations and are omitted for the sake of conciseness.

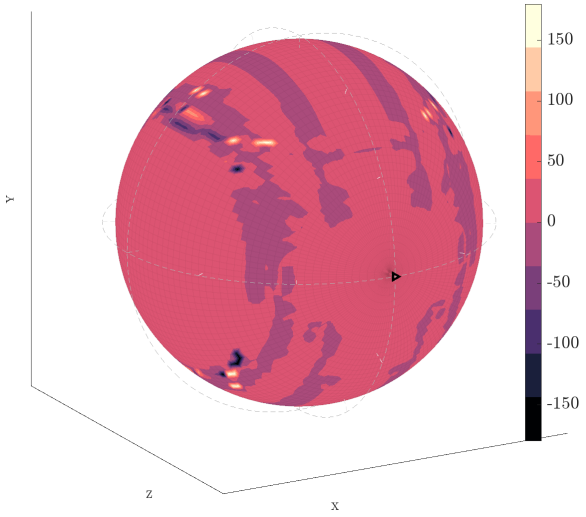

Fig. 8: $\phi_{dir}(f,\theta,\varphi)$ difference at 10°C between balloons computed with fixed speed and a temperature dependent model, f = 16.8kHz.

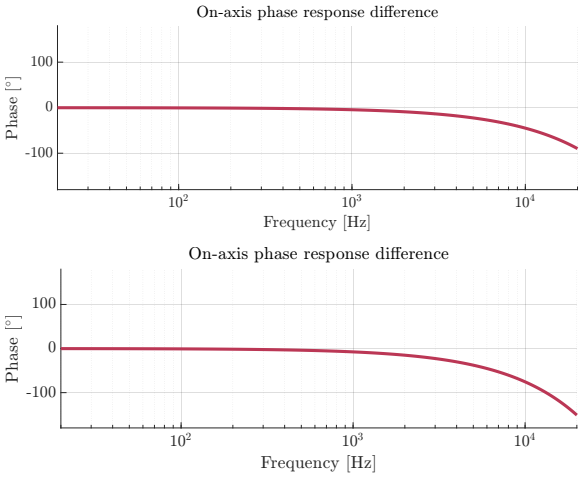

Fig. 9: $\phi_{on-ax}(f)$ difference at 30%RH (top) and 70%RH (bottom) between balloons computed with fixed speed and a temperature dependent model.

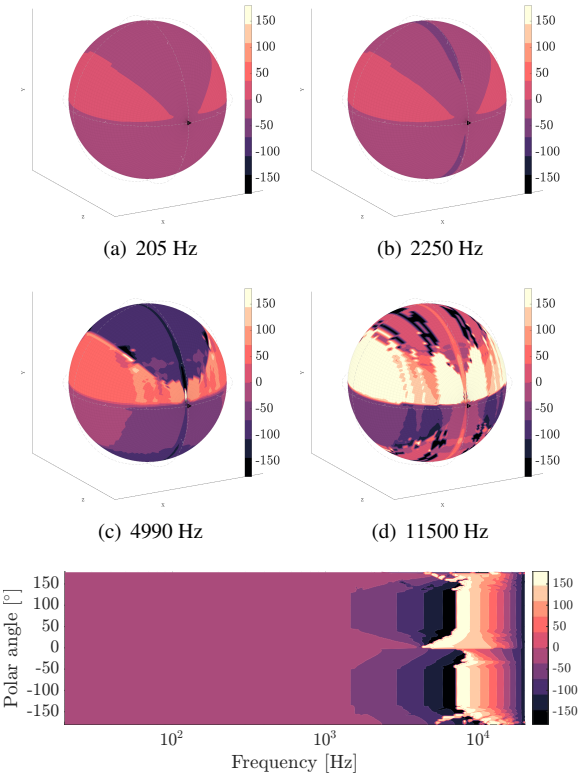

Fig. 10: $\phi_{tot}(f,\theta,\varphi)$ differences between balloons computed using a fixed sound speed and a temperature-dependent model, assuming 5°C difference between the cylinder measurements.

4.2 Cylinders measured under different ambient conditions

It is also interesting to illustrate the effect of employing an improper sound speed value when the two cylindrical datasets are measured under different environmental conditions. For instance, this could be the case of two high-resolution datasets, which may take several hours to measure, acquired on different parts of the day or even consecutive days. In this scenario, even moderate changes in the sound speed value used in the model can have dramatic effects on the final phase response of the balloon. The impact of an uncompensated, 5°C discrepancy between the orthogonal cylindrical datasets (RH set to 50%, 20°C for the first cylinder and 25°C for the second) with respect to the datasets compensated using the ambient parameters acquired during the measurement is shown by $\phi_{tot}(f,\theta,\varphi)$ in Fig.10. Similarly, Fig.11 show the effects given by 10°C difference between the measurement conditions of the cylinders.

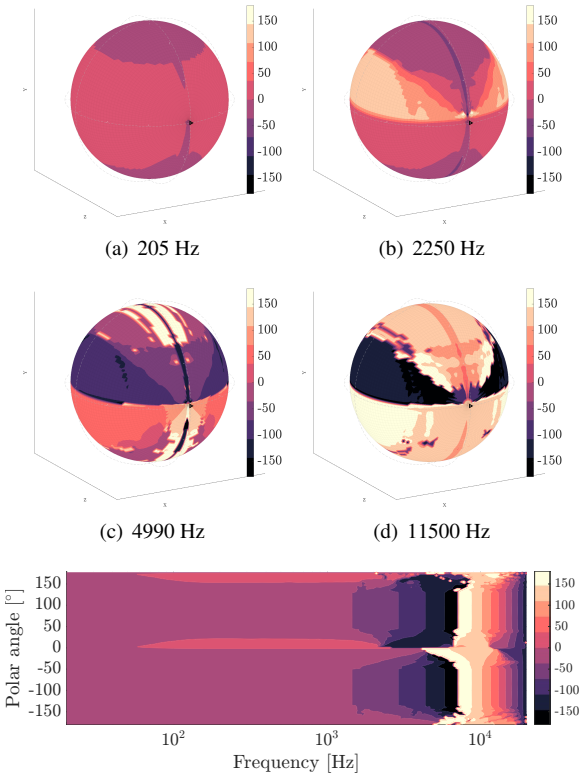

(a) 205 Hz (b) 2250 Hz

(c) 4990 Hz (d) 11500 Hz

(e) Vertical polar

Fig. 11: $\phi_{tot}(f,\theta,\varphi)$ differences between balloons computed using a fixed sound speed and a temperature-dependent model, assuming 10°C difference between the cylinder measurements.

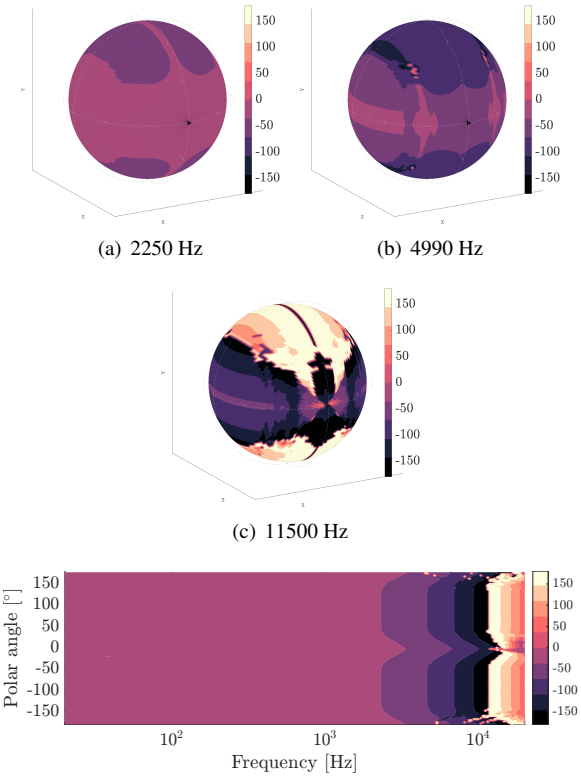

(a) 2250 Hz (b) 4990 Hz

(c) 11500 Hz

(d) Vertical polar

Fig. 12: $\phi_{tot}(f,\theta,\varphi)$ differences between balloons computed using a fixed sound speed and a temperature-dependent model, assuming a uniform temperature rise of 5°C throughout the measurement.

4.3 Temperature rising between each horizontal measurement

As a final case study, the temperature is set to rise from 20°C to 25°C in equal steps throughout the whole measurement process (RH fixed to 50%). More specifically, the speed of sound is unvaried for measurements in each pair of horizontal disk-datasets recorded by both microphones at the same time, and it is increased in all subsequent pairs of measurements that compose each of the orthogonal cylinders. This also resembles a real-life scenario in which the environmental parameters could change continuously as the measurement progresses. As in the previous case, comparing the phase response of the so-obtained directivity balloon with the one compensated employing the measured ambient parameters underlines that the observed differences are still direction-dependent. As shown in Fig.12, this could lead to non-negligeable errors in the proximities of the on-axis direction, where the magnitude of the radiated field is usually high.

5 Conclusions

The cylinder measurement method can provide the full-sphere directivity balloon of a loudspeaker with the aid of limited equipment, compared to measurement procedures involving arcs of microphones around the loudspeaker, and restricts the automated movements of the DUT to a rotation on the horizontal plane and a vertical translation only. The two cylindrical measurements are then projected to a unitary-radius sphere and interpolated by means of spherical interpolation processes. However, the disk-measurements within

the cylinders and the cyliders themselves are acquired sequentially, thus the importance of using a refined ambient parameter-dependent model for the propagation speed of sound is highlighted, as to compute accurate phase responses of the directivity data. As the sound speed varies with changes in quantities such as temperature, relative humidity and atmospheric pressure, careful propagation-compensation methods should be used, employing ambient parameters values recorded between each disk-measurement. Such shrewdness is also demonstrated to be essential in order to grant the repeatability of the measurement results, if the data acquisition is performed at different times of the day, month or year, in changing environmental conditions.

6 Acknowledgements

The author expresses his sincere gratitude to the NEXO company (`https://www.nexo-sa.com`) for its support. Additionally, the author would like to thank Daniele Ponteggia and Joerg Panzer for the interesting discussions and their helpful comments.

References

[1] Catala Iborra, V. M. and Li, F. F., "DSP Loudspeaker 3D Complex Correction," *146th AES Convention*, 2019.

[2] Meyer, D. G., "Development of a Model for Loudspeaker Dispersion Simulation," *72th AES Convention*, 1982.

[3] Jacob, K. D. and Birkle, T. K., "Prediction of the Full-Space Directivity Characteristics of Loudspeaker Arrays," *J. Audio Eng. Soc*, 38, pp. 250–259, 1990.

[4] Seidel, F. and Staffeldt, H., "Frequency and Angular Resolution for Measuring, Presenting, and Predicting Loudspeaker Polar Data," *J. Audio Eng. Soc*, 44, pp. 555–568, 1996.

[5] AES standard on acoustics. AES56-2008 (r2019), "Sound source modeling - Loudspeaker polar radiation measurements," 2019.

[6] Struck, C. J. and Temme, S. F., "Simulated Free Field Measurements," *93rd AES Convention*, 1992.

[7] Ponteggia, D., "Automated Balloon Measurements with CLIO 10," Technical report, AUDIOMATICA, 2009.

[8] Feistel, S., *Modeling the Radiation of Modern Sound Reinforcement Systems in High Resolution*, Logos Verlag Berlin GmbH, 2014.

[9] Williams, E. G., *Fourier Acoustics*, Academic Press, 1999, ISBN 978-0-12-753960-7.

[10] Fazi, F. M., Brunel, V., Nelson, P. A., Hörchens, L., and Seo, J., "Measurement and Fourier-Bessel analysis of loudspeaker radiation patterns using a spherical array of microphones," *124th AES Convention*, 2008.

[11] Hughes, C., "How Accurate is Your Directivity Data?" 2005.

[12] Panzer, J. and Ponteggia, D., "Inverse Distance Weighting for Extrapolating Balloon-Directivity-Plots," *131st AES Convention*, 2011.

[13] Bru, M., "Cylinder Measurement Method for Directivity Balloons," *149th AES Convention*, 2020.

[14] Beranek, L., *Acoustics*, The Acoustical Society of America, 1954.

[15] Feistel, S., Ahnert, W., Hughes, C., and Olson, B., "Simulating the Directivity Behavior of Loudspeakers with Crossover Filters," *123rd AES Convention*, 2007.

[16] Baird, J. E. and Meyer, P. S., "The Analysis, Interaction, and Measurement of Loudspeaker Far-Field Polar Patterns," *106th AES Convention*, 1999.

[17] Bohn, D. A., "Environmental Effects on the Speed of Sound," *J. Audio Eng. Soc*, 36, pp. 223–231, 1988.

[18] Cramer, O. P., "The variation of the specific heat ratio and the speed of sound in air with temperature, pressure, humidity, and CO2 concentration," *Journal of the Acoustical Society of America*, 93, pp. 2510–2516, 1993.

[19] Snyder, J. P., *Flattening the Earth : Two Thousand Years of Map Projections.*, University of Chicago Press, 1993.